Efficiency of Hydrogen Recovery from Reformate with a Polymer Electrolyte Hydrogen Pump

Ahmed Abdulla, Kathryn Laney, Miriam Padilla, Sankaran Sundaresan, and Jay Benziger
Chemical and Biological Engineering Dept., Princeton University, Princeton, NJ 08544

DOI 10.1002/aic.12406
Published online September 29, 2010 in Wiley Online Library (wileyonlinelibrary.com).

The energy efficiency of hydrogen recovery from mixtures of CO_2, H_2O, and H_2 by a polymer electrolyte hydrogen pump (PEHP) has been evaluated. The PEHP pumps protons across the polymer electrolyte, producing >99.99% pure H_2 and a concentrated CO_2 stream. Single stage PEHP experiments recovered 65% of the hydrogen with an energy efficiency of 50%. The energy efficiency is limited by hydrogen mass transport across the porous gas diffusion electrode. The mass transport resistance for hydrogen increases as H_2 is depleted from the CO_2/H_2 mixture by the PEHP. Analysis shows that a multistage PEHP with fixed applied potential difference can recover >90% of the hydrogen with an energy efficiency of 75%, whereas a novel multistage PEHP design with a programmed voltage profile can achieve >90% energy efficiency with >98% hydrogen recovery. © 2010 American Institute of Chemical Engineers *AIChE J,* 57: 1767–1779, 2011

Keywords: hydrogen, reformate purification, electrochemical separations, carbon dioxide removal

Introduction

Energy recovery from coal with carbon sequestration is a critical technology to reduce atmospheric carbon emissions in the next 20 years. Efficient separation of hydrogen from carbon dioxide is essential for successful integrated coal gasification and carbon capture. Steam reforming followed by the water gas shift reaction converts the coal into reformate, primarily CO_2, H_2O, and H_2.[1,2] After H_2/CO_2 separation, the H_2 can be used as a fuel, and the CO_2 can be sequestered. Hydrogen is a clean versatile fuel that can be used in several different energy conversion technologies; it can be combusted in gas turbines or be electrochemically converted to electricity in fuel cells.[3,4] Hydrogen can also be sent via pipelines from remote locations where the reforming and sequestration are done to the points of use. As a fuel, hydrogen only emits water vapor into the atmosphere at the point of use, whether used in a turbine or a fuel cell.

"Hydrogen from Coal Multi-Year R&D Plan" of the US Department of Energy (DOE) presents in detail the expected improvements in gasification technology that will make integrated coal gasification and carbon sequestration a commercially viable option for hydrogen production in the future.[5] Because of the large amounts of CO_2 that are produced in this process, efficient methods for separating CO_2 and H_2 are necessary. The DOE is running a carbon sequestration R&D initiative parallel to the "Hydrogen from Coal" program to use coal without contributing to global warming.[6] Current sequestration methods cost between $100 and $300 per ton of carbon emissions are avoided, and the goal is to reduce these costs to under $10 per ton,[6] so there is a long way to go before carbon sequestration can be adopted on a large scale.

Steam reforming of coal followed by the water gas shift reaction generates a mixture of hydrogen and carbon dioxide ($CO_2/H_2 = 0.5$ for coal $CO_2/H_2 = 0.25$ for natural gas),

Correspondence concerning this article should be addressed to J. Benziger at benziger@princeton.edu.

water vapor, and lesser amounts of impurities including carbon monoxide (CO/CO_2 0.01–0.1), low molecular weight hydrocarbons, and sulfur compounds. ''Clean energy'' should recover a pure hydrogen product from the reformate stream.[7,8] State-of-the-art technology emphasizes CO_2 removal rather than hydrogen recovery. Traditional approaches use alkaline or amine scrubbing of the CO_2. The scrubbing solutions must be regenerated by heating them to desorb the CO_2. The heat input for CO_2 desorption is substantial and reduces the overall energy efficiency of the process to ~75%.[1,8] Furthermore, the impurities in the reformate stream are left mixed with the H_2 stream, which requires a second purification step to recover the hydrogen.

Pressure swing adsorption is an alternative method to remove the CO_2 from reformate by adsorption onto a basic metal oxide.[9–13] Other methods of purifying hydrogen include cryogenic distillation[14,15] and membrane separation techniques.[16–26] Cryogenic methods are not very energy efficient. Membrane separators include palladium and microporous silica materials; the present membranes are too costly to be used on a large scale.

Other separation methods are used to remove the trace amounts of carbon monoxide, hydrocarbons, and sulfur compounds that remain in the hydrogen after CO_2 removal. The most significant impurity is carbon monoxide, which occurs at concentrations of 0.1–1% in reformate streams. CO can be converted to CO_2 using selective oxidation catalysis at the front end of the hydrogen recovery.[27–32] This technology has been demonstrated for treating CO impurities in the hydrogen feed to PEM fuel cells.

We report here the efficiency of recovery of hydrogen from H_2-CO_2 mixtures by electrochemical pumping. The polymer electrolyte hydrogen pump (PEHP) consists of a proton conducting polymer electrolyte sandwiched between two porous electrodes as shown in Figure 1. Reformate gas stream containing H_2 is fed to the anode. Voltage is applied across the cell, oxidizing H_2 to protons and electrons at the anode. The protons are transported across the polymer electrolyte membrane to the cathode, where they are reduced producing hydrogen. The pumping is done at low potentials where CO_2 and H_2O are electrochemically unreactive; only hydrogen is pumped across the electrolyte producing a pure hydrogen stream at the cathode. The PEHP acts both as a separator unit and as a pump; a small increase in the applied potential difference can pressurize the hydrogen stream at the cathode. This is an advantage to permselective membranes where the separation is pressure driven and the hydrogen product is recovered at reduced pressure.

Several applications of PEHPs have been reported in the literature. The PEHP as a compressor has been studied[33]; the PEHP allows for energy efficient pressurization of hydrogen. More recently, PEM fuel cells have been combined with electrochemical pumps for the purpose of hydrogen recirculation in fuel cell stacks.[34]

The idea of using PEHPs for the purpose of purification of mixed streams was pioneered in the 1980s by Sedlak et al.[35] The concept was recently revived and several papers have been written over the past 2–3 years. Gardner and Ternan demonstrated the feasibility of recovery of hydrogen from H_2/CO_2 mixtures with and without CO contamination.[36] They demonstrated that pulsing the voltage to periodically oxidize adsorbed CO could mitigate the problem of CO contamination. The maximum current densities observed by Gardner and Ternan were ~0.2 A/cm^2. Casati et al. reported the operation of a PEHP for separating H_2 from H_2/N_2 mixtures.[37] They showed that the recovery increased with applied potential difference and the coefficient of performance (defined as the ratio of hydrogen produced to hydrogen consumed) decreased with applied potential difference. Casati et al. suggested that there should be optimum energy efficiency for separation, but they did not identify the functional dependence of the optimum on process parameters. Both Gardner and Ternan and Casati et al. used Nafion membrane-based PEHPs. Recently, Benicewicz and co-workers demonstrated the use of a polybenzimidazole membrane in the PEHP.[38] The PBI membrane operated at higher temperature (~160°C) than the Nafion membranes (~25–70°C). Benicewicz et al. determined that the efficiency of hydrogen pumping was highest with pure hydrogen (as expected); they also examined the effects of temperature and voltage on mitigating the deleterious effect of carbon monoxide. Unfortunately, they did not report mass balances, so it was not possible to identify the energy efficiency for hydrogen separation. The previous studies appeared to focus on the problem of impurities in the reformate feed. Benicewicz is also involved with a company that produces a PEHP using the PBI membrane technology; however, the specifications of the operating efficiency are not available.[39,40] None of the previous studies analyzed the overall energy efficiency of operation of their PEHPs. When efficiency was considered, the studies defined energy efficiency as net energy recovered divided by the total energy recovered at the cathode. The authors failed to account for the energy lost in the hydrogen leaving the anode. Those studies demonstrated the principle of PEHP operation, but did not examine the engineering

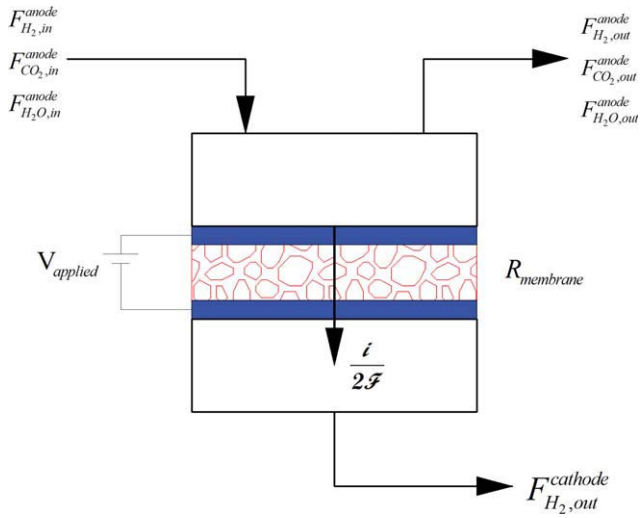

Figure 1. Representation of a polymer electrolyte hydrogen pump (PEHP).

A simulated reformate of $H_2/CO_2/H_2O$ is fed to the fuel cell at the anode. Hydrogen is oxidized at the anode into protons and electrons. The protons are pumped across the membrane, whereas their electrons are transmitted through an external circuit. The protons are reduced at the cathode producing a purified H_2 stream. [Color figure can be viewed in the online issue, which is available at wileyonlinelibrary.com.]

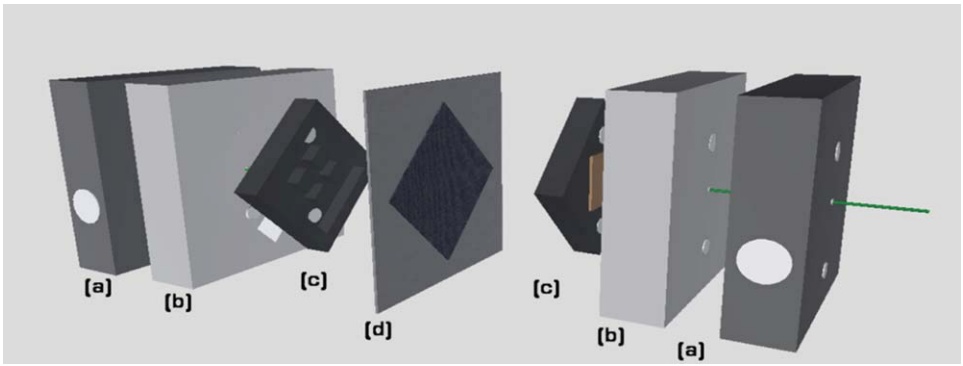

Figure 2. An exploded view of the assembled polymer electrochemical hydrogen pump.

The MEA (d) is sandwiched between the two graphite channel-less self-draining electrodes (c). A Cu plate is pressed against the back of the graphite plates as shown on the right hand side graphite plate (c). These are embedded into Teflon plates (b), which are supported by stainless steel heat sinks (a) with cartridge heaters. [Color figure can be viewed in the online issue, which is available at wileyonlinelibrary.com.]

aspects of sizing and optimize throughput for hydrogen recovery.

In this article, we report the development of a novel multistage PEHP to achieve very high hydrogen recovery and energy efficiency. We first describe the experimental results on hydrogen recovery and energy efficiency from $H_2/CO_2/H_2O$ mixtures obtained in a single-stage Nafion-based PEHP, where the energy efficiency was found to be limited to circa 50%. These results are then analyzed using a simple mathematical model to expose the role of resistance for hydrogen transport across the porous electrode at the anode in limiting energy efficiency. Armed with this understanding, we then evaluate the performance characteristics of multistage PEHPs. We demonstrate that a multistage PEHP operating at fixed voltage can increase the energy efficiency to circa 75%, whereas a multistage PEHP with a programmed voltage profile can recover >98% of the hydrogen from a reformate stream at >92% energy efficiency, which far exceeds those achievable by other separation methods that focus on extracting CO_2 from the mixtures.

We have not considered trace impurities, such as CO, H_2S, COS, and so forth that are present in reformate stream. The intent of this study is to assess the highest possible efficiency of H_2 purification from clean H_2/CO_2 mixtures attainable through PEHPs; unless the PEHP system operating with clean $H_2/H_2O/CO_2$ is more efficient than existing technologies for CO_2 separation, it would be meaningless to pursue any further development of the PEHP. Hence, our emphasis has been to identify the system parameters relevant to energy efficiency and explore the overall energy efficiency for different designs.

Experimental

The PEHP used in this investigation was based on the one-dimensional differential or stirred tank reactor (STR) Polymer Electrolyte Membrane (PEM) fuel cell developed at Princeton.[41] The STR design replaces the serpentine gas flow channels seen in most commercial applications with an open plenum that allows for thorough gas mixing at the anode and cathode. The open plenum has four distributed pillars of equal height that apply pressure on the membrane-electrode-assembly (MEA) and act as current collectors once the fuel cell's connecting bolts are tightened. The membrane electrolyte assembly has a surface area of 1.9 cm^2 and a plenum height of 1.6 mm. Injection and exhaust ports were drilled into each graphite electrode angled for gravity-assisted drainage of liquid from the plenums.

The MEA was comprised of two carbon cloth E-TEK gas diffusion media with a microporous layer on one side (DeNora, NJ) and a catalyst coated Nafion® 115 membrane (127 μm thick Nafion membrane from Ion Power, DE). The catalyst coating was applied by air-brushing a suspension of 20 wt % Pt/C catalyst (Sigma-Aldrich) and solubilized Nafion in methanol. The catalyst loading was 0.4 mg Pt/cm^2. Nafion membranes were prepared for use by boiling in 3% H_2O_2/water, deionized water, 1 M H_2SO_4, and deionized water for 1 h per step. Water drops were tamped from the membrane and catalyst layers were applied to both sides of the membrane by air brushing. After applying the catalyst coating, the membranes were annealed in a vacuum oven at 70°C for 2 h and then stored in a sealed glass container at 100% RH and room temperature until use.

The catalyst-coated membrane was positioned between the silicon gaskets and gas diffusion layers (GDLs) and then placed between the two graphite plates machined with the plenum and pillars. The graphite plates were press fit into two Teflon plates placed between two stainless steel plates. The temperature of the cell was controlled by cartridge heaters mounted in cylindrical ports drilled in the stainless steel plates. Figure 2 is an exploded 3D model of the assembled PEHP cell.

Wires were soldered onto copper plates, which in turn were glued (acrylic cement mixed with silver powder) to each electrode. The lead wires from the fuel cell connect to the external circuit through which the driving voltage for hydrogen pumping was applied.

The PEHP assembly is placed in a thermally insulated box, along with a gas humidifier, as illustrated in Figure 3. H_2, CO_2, and N_2 gases from standard purity industrial cylinders were metered through Aalborg® 0–50 mL/min mass flow controllers. The H_2 and CO_2 flow rates were set to achieve a desired composition, mixed in a T-junction and sent to the humidifier within the insulating box. The humidifier's water level was monitored and maintained manually. Humidified H_2/CO_2 was fed into the anode compartment of the PEHP. The effluents from the anode and cathode were

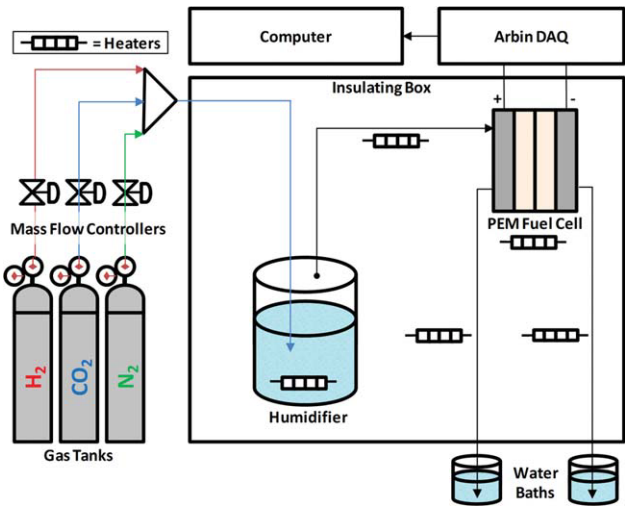

Figure 3. A schematic of the setup, showing the gas delivery apparatus, as well as the insulating box containing the gas humidifier and the PEM fuel cell assembly.

Temperature control techniques are used at the humidifier, fuel cell, anode inlet, anode outlet, and cathode outlet. [Color figure can be viewed in the online issue, which is available at wileyonlinelibrary.com.]

either collected in inverted graduated cylinders filled with water to measure the integrated gas flows or run through soap bubble meters to measure flow rates; the gas flow rates allowed us to close the mass balances with less than 3% error in all experiments. In all the experiments reported here, the total pressure at both the anode and cathode was 1 bar (within 10 cm of H_2O). The PEHP cartridge heaters and the humidifier heater were connected to digital controllers (Omega) to maintain the desired temperatures. All the gas flow lines to and from the PEHP cell were heat traced with heating tapes connected to variacs to avoid liquid condensation in the lines. Relative humidity sensors (SENSIRON) were placed in tees at the outlets from the PEHP cell.

The fuel cell's external circuit wires were connected to an Arbin data acquisition system running the Arbin's MSTAT4+ software. The Arbin is a capable of running schedules that involve current ramps, current holds, voltage ramps, voltage holds, and membrane R_{int} checks using the current-interrupt method. Arbin schedules were programmed for current measurements for 1 h at fixed applied potential differences. A current interrupt measurement was made at the beginning and end of each potentiostatic measurement to determine the internal resistance of the membrane. The voltage was ramped in steps of 0.1 V from 0 to 0.8 V. Tests were carried out with water saturated feeds, CO_2/H_2 feed ratios of 0, 0.2, 0.33, 0.5, 1.0, and 2.0, flow rates of 16–48 mL/min (2.9–17.2 $\times 10^{-6}$ mol/cm^2 MEA s) and temperatures of 50 and 70°C.

CO_2 concentrations in the anode and cathode outlets were measured by passing fixed volumes of 50 mL through Sensidyne precision gas detector tubes (GDTs). The anode effluent was passed through a 126UH tube to measure CO_2 concentrations of 5–50 vol % CO_2. The cathode effluent was tested with a 126 SG model to measure a range of 0.02–1.4 vol % CO_2. GDTs are graduated tubes containing a fixed bed of reactant that on contact with CO_2 changes color. A total of 50 mL of the outlet gas was passed through the appropriate tube, and the volume of CO_2 in that sample was determined from the color change of the GDTs.

Results

A sample set of experimental data is shown in Figure 4 for a total dry flow rate of 24 mL/min (8.6 $\times 10^{-6}$ mol/cm^2/s) at 50°C. The applied potential difference was stepped up from 0 to 0.8 V in increments of 0.1 V, and the current was measured for a 1-h period while holding the voltage fixed. The CO_2/H_2 ratio of the feed is indicated. $(C/H)_{in} = 0$ is a feed of hydrogen and water vapor ($P_w = P_w^0$) at a total pressure (P_T) of 1 bar. The partial pressure of water in the anode feed is equal to the saturation pressure at 50°C (0.138 bar), and the hydrogen pressure is the difference between the total pressure and water vapor pressure ($P_H = 1.0 - 0.138 = 0.862$ bar). $(C/H)_{in} = 0.5$ corresponds to the typical composition from coal gasification. The feed rate and compositions of the feed are given by temperature, $(C/H)_{in}$ ratio and dry feed molar flow rate (F_{dry}) as given in Eqs. 1.

$$\begin{aligned}
&\text{Molar Feed Rate (mol/s)} \quad F_{\text{dry}}/\left(1 - P_w^0/P_T\right)\\
&\text{Mole Fraction Water anode in} \quad x_w = P_w^0/P_T\\
&\text{Mole Fraction } H_2 \text{ anode in} \quad x_H = \frac{\left(1 - P_w^0/P_T\right)}{\left(1 + (C/H_{in})\right)}\\
&\text{Mole Fraction } CO_2 \text{ anode in} \quad x_{CO_2} = \frac{\left(1 - P_w^0/P_T\right)(C/H)_{in}}{\left(1 + (C/H)_{in}\right)}
\end{aligned} \tag{1}$$

The membrane resistance was determined from current interrupt measurements; the areal resistivity was constant to within 10% (e.g., 0.45 $\pm$ 0.05 Ω cm^2) over the course of an experiment such as shown in Figure 4; the resistivity of

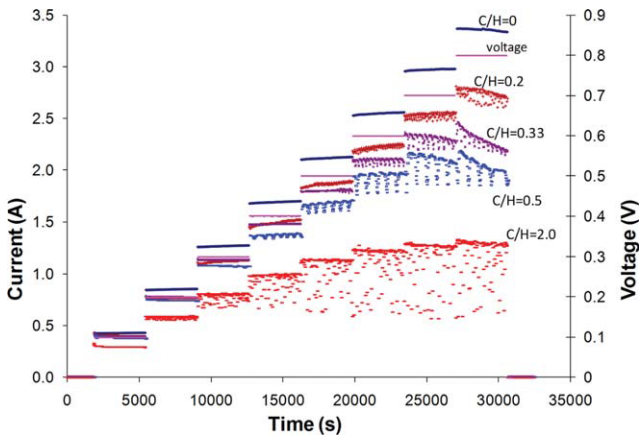

Figure 4. Sample of experimental data for current as a function of applied potential difference at different $(C/H)_{in}$ ratios with a water saturated feed at 50°C.

Total dry flow was fixed at 24 mL/min with an MEA area of 1.9 cm^2 (flow rate = 8.6 $\times 10^{-6}$ mol/cm^2/s). [Color figure can be viewed in the online issue, which is available at wileyonlinelibrary.com.]

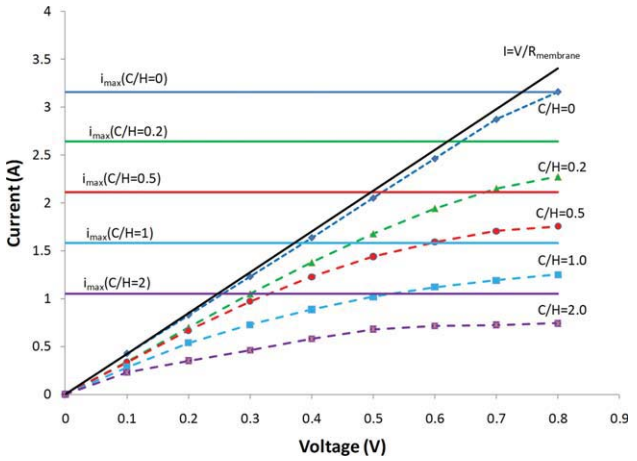

Figure 5. Average current as a function of applied potential difference at different $(C/H)_{in}$ ratios with a water saturated feed at 50°C.

The horizontal lines are the stoichiometric limits to the current at the different $(C/H)_{in}$ ratios. [Color figure can be viewed in the online issue, which is available at wileyonlinelibrary.com.]

different MEAs varied from day to day within the range of 0.45–0.75 Ω cm^2. The relative humidity at the anode was always 100%, and the relative humidity at the cathode was always >85%. We never saw evidence of reduced relative humidity or increased membrane resistivity from drying.

At $(C/H)_{in} = 0$, the current increased almost linearly with applied potential difference over the range of 0–0.8 V, consistent with the proton current being limited by the ohmic resistance of the membrane over the entire applied potential difference range. To simplify the data presented in Figure 4, the average current during each voltage hold was evaluated and plotted against the applied potential difference in Figure 5. The linear increase of current with applied potential difference at $(C/H)_{in} = 0$ is seen more clearly in Figure 5. Horizontal lines plotted in Figure 5 are the limiting currents based on the molar hydrogen feed to the hydrogen pump as given by Eq. 2.

$$i_{max} = \frac{2\mathcal{F}F_{dry}}{\left(1 + (C/H)_{in}\right)} \tag{2}$$

Figures 4 and 5 both show that the current increased linearly with applied potential difference at low voltages for all $(C/H)_{in}$ ratios. The current reached a limiting value that was less than the stoichiometrically limited current ($i < 2F^{in}_{H_2}/\mathcal{F}$) as the applied potential difference was increased. Hydrogen oxidation at the anode catalyst layer is fast when the applied potential difference is large depleting the hydrogen at the anode catalyst layer, which results in the proton current becoming limited by hydrogen mass transport across the porous GDL. This is analogous to mass transport limited reaction on a catalyst surface at high temperature.

As the gases are well mixed in both the anode and cathode plenums, the gas composition in the anode plenum can be determined by mass balances (the mass balance equations are given later in Eqs. 7 and 8). Figure 6 plots the current as a function of the mole fraction of hydrogen at the anode outlet at 50 and 70°C for different applied potentials; this graph summarizes all the different flow rates and different $(C/H)_{in}$ ratios. Two transport regimes are evident from the data in Figure 6. At constant applied potential difference, the current initially increases linearly with hydrogen mole fraction, x_{H2}. As the hydrogen mole fraction increases, the current reaches a limiting value. The limiting current increases with applied potential difference. As explained in detail below, the increase in current with hydrogen mole fraction at small x_{H2} corresponds to the current being limited by hydrogen mass transport across the GDL (where the hydrogen concentration approaches zero at the anode catalyst layer). At higher hydrogen mole fraction, the mass transport across the GDL is sufficiently fast, so the concentration gradient across GDL is small, and the proton current across the membrane is limited by applied potential difference. The slope of the linear increase in current with hydrogen mole fraction is equal to the effective mass transport coefficient of hydrogen across the GDL, $k_m = 4.6$ A/bar cm^2 $= 2.4 \times 10^{-5}$ mol/bar cm^2. The data suggest that the hydrogen mass transport coefficient was insensitive to changes in temperature between 50 and 70°C.

The data in Figure 4 showed an unusual feature. At applied potential differences above 0.3 V, the current manifested regular oscillations; these are highlighted in Figure 7 where the time between 20,000 and 25,000 s has been blown up. The magnitude of the oscillations increased with increasing (C/H) ratio, becoming chaotic at the highest (C/H) ratio. We suggest these oscillations are due to water condensing in the anode. When hydrogen is removed from the water saturated feed at the anode, the vapor becomes supersaturated with water and liquid condenses. At higher currents, accompanying higher applied potential difference, more water condenses and the more pronounced are the oscillations. Even though we used a self-draining cell design, the water

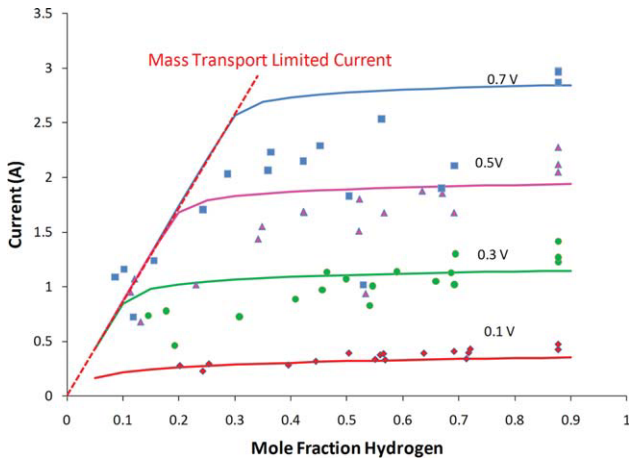

Figure 6. Current in the PEHP as a function of anode outlet hydrogen concentration and applied potential difference.

Data from different flow rates, inlet compositions and at temperatures of 50 and 70°C are summarized. The solid lines are calculated from the model with values of $k_m = 2.4 \times 10^{-5}$ mol/bar cm^2 s and $\rho_{membrane} = 0.47$ Ω cm^2. [Color figure can be viewed in the online issue, which is available at wileyonlinelibrary.com.]

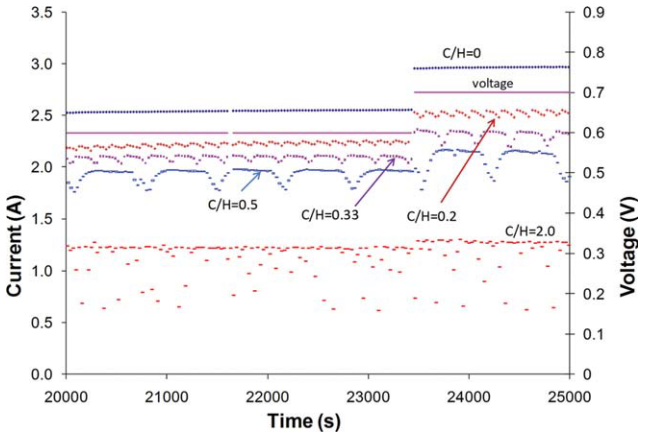

Figure 7. Blow up of the time period between 20,000–25,000 s from Figure 4.

This illustrates the regulator current oscillations that occur due to the accumulation of liquid water in the anode of the PEHP. [Color figure can be viewed in the online issue, which is available at wileyonlinelibrary.com.]

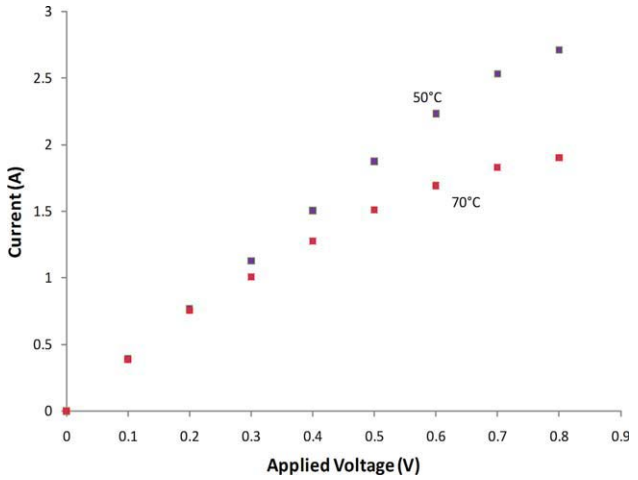

Figure 8. Effect of temperature on the current in the PEHP.

The PEHP feed was 24 cm^3/min with a $(C/H)_{in}$ ratio of 0.5. [Color figure can be viewed in the online issue, which is available at wileyonlinelibrary.com.]

appeared to form drops that accumulated at the outlet to the cell. The outlet is a 3-mm hole drilled through a graphite plate. A small pressure (100 Pa) is needed to push the water drops through the hydrophobic graphite hole. As the liquid accumulates near the outlet of the cell, part of the MEA becomes inactive causing a drop in the current. The liquid accumulation at high currents causes part of the electrode to become inactive, this also causes the decline in the current with time at high voltages seen in Figure 4.

The second effect of water vapor is that it dilutes the hydrogen/carbon dioxide gas mixture. The water partial pressure is determined by the vapor pressure of water at the temperature of the PEHP cell; the sum of the hydrogen and carbon dioxide pressures is equal to the total pressure less the water vapor pressure. Increasing the temperature of the PEHP at a fixed total pressure increases the water vapor pressure reducing the partial pressures of H_2 and CO_2. The reduction in hydrogen partial pressure due to increased water vapor pressure caused a reduction in the current as shown in Figure 8 where the current as a function of applied potential difference at 50° and 70° are compared for the same $(C/H)_{in}$ ratio and same dry feed rate. The current is reduced at the higher temperature because the hydrogen pressure is effectively reduced, which results in greater mass transport resistance across the GDL.

As a separation technique the figures of merit of the PEHP are: (1) the separation efficiency; (2) the energy efficiency; and (3) product purity. The hydrogen product obtained in our study was very pure; there were <200 ppm CO_2 in the hydrogen product stream, which was at our detection limit. The separation efficiency is the fraction of hydrogen feed to the anode that flows out the cathode. The energy efficiency is equal to the energy content of the product hydrogen less the energy expended on separation divided by the energy content of the hydrogen in the feed. The energy content of hydrogen was assumed to be the heat of combustion of the hydrogen. These separation and energy efficiencies are defined in Eqs. 3 and 4.

$$\text{Separation Efficiency} = \frac{i}{2\mathcal{F}F^{\text{anode}}_{H_2,\text{in}}} \tag{3}$$

$$\text{Energy Efficiency} = \frac{\frac{i}{2F}\Delta H_{\text{combustion}} - iV_{\text{applied}}}{F^{\text{anode}}_{\text{H}_2,\text{in}}\Delta H_{\text{combustion}}} \tag{4}$$

The separation and energy efficiencies for the PEHP operating at 50°C, total flow of 24 cm^3/min and two different $(C/H)_{in}$ ratios as functions of the applied potential difference are shown in Figure 9. Hydrogen recovery increases with applied

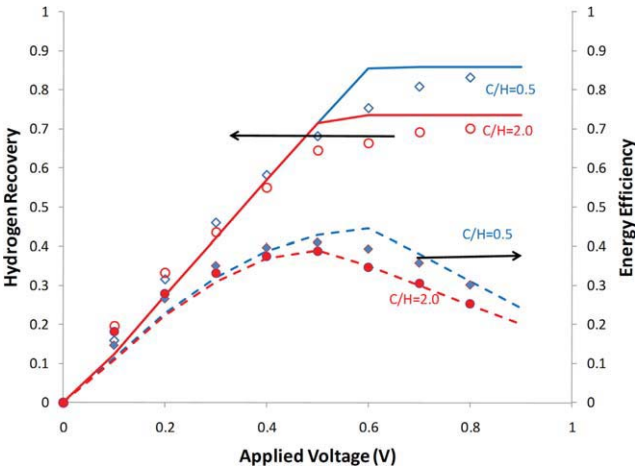

Figure 9. Hydrogen recovery and net energy efficiency for H_2 recovery from $H_2/CO_2/H_2O$ streams in the polymer electrochemical pump as a function of applied potential difference and C/H inlet ratio.

The points are the experimental data at 50°C, water saturated feed, 24 mL/min $H_2 + CO_2$ feed with $(C/H)_{in}$ ratio as specified. The solid lines (recovery) and dashed lines (energy efficiency) are based on the model presented below. The model calculations were based on the determined values of k_m and ρ_{mem} for the 1.9 cm^2 PEHP at 50°C, 1 bar, 24 mL/min dry inlet flow, with $(C/H)_{in}$ per experiment. [Color figure can be viewed in the online issue, which is available at wileyonlinelibrary.com.]

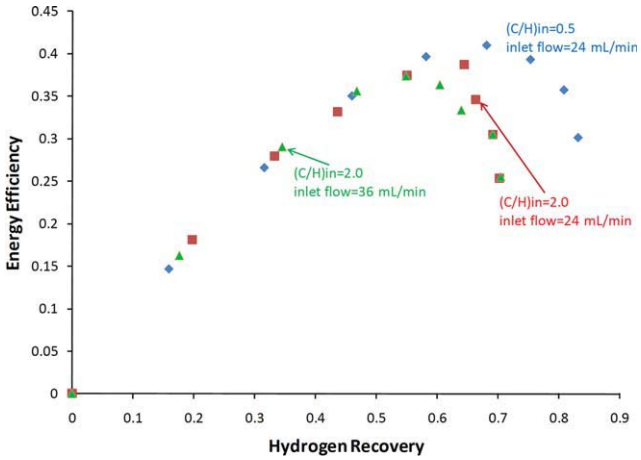

Figure 10. Energy Efficiency as a function of hydrogen recovery from $H_2/CO_2/H_2O$ mixtures at different $(C/H)_{in}$ ratios an different inlet flow rates.

[Color figure can be viewed in the online issue, which is available at wileyonlinelibrary.com.]

potential difference and levels out at a maximum recovery; the greater the $(C/H)_{in}$ ratio the lower the maximum recovery. The energy efficiency goes through a maximum with applied potential difference; the maximum energy efficiency is ~45%, achieved at an applied potential difference of ~0.5 V.

Figure 10 presents the data from Figure 9 in terms of the figures of merit for the separation process, plotting energy efficiency as a function of hydrogen recovery. A third data set not shown in Figure 9 is included to show how the energy efficiency for the same inlet composition, $(C/H)_{in} = 0.5$, changes with flow rate. Energy efficiency goes through a maximum with hydrogen recovery, and the maximum energy efficiency is reduced at higher flow rates. At low hydrogen recovery, the energy efficiency is independent of $(C/H)_{in}$ ratio and flow rate; this is the operating regime where the current is limited by the applied potential difference. The energy efficiency increases with recovery because less hydrogen is lost in the waste stream (the CO_2 stream) as recovery increases. At high hydrogen recovery, the current is limited by hydrogen mass transport across the anode GDL. When mass transport across the GDL is rate limiting increasing the potential difference does not increase the current. Increasing the voltage in the H_2 gas transport limited regime causes greater ohmic losses without any increased current, which decreases the energy efficiency. The maximum energy efficiency occurs at the transition between proton transport limited current and mass transport limited current.

Discussion

Hydrogen purification from reformate mixtures with PEHPs has been demonstrated by several previous investigators.[33,34,36–38] Those studies focused on the feasibility of the hydrogen pump for purification; only Casati et al. [37] performed any analysis on the recovery and efficiency of the process. They reported an increase in the hydrogen recovery with applied potential difference and they also observed that the energy efficiency decreased with applied potential difference (Casati et al. defined a coefficient of performance as a measure of energy efficiency). Casati et al. showed an optimum recovery as a function of space time, but they did not see an optimum energy efficiency. They did not determine the relationship between composition on the recovery or efficiency. Both Casati et al. and Gardner and Ternan defined energy efficiency as the net energy in the cathode stream $((F^{cathode}_{H2,out} \Delta H_{H_2,combusion} - iV_{applied})/F^{cathode}_{H2,out} \Delta H_{H_2,combusion})$. They did not account for the energy of the hydrogen lost in the effluent of the anode stream.

The previous studies of PEHPs used complex flow field in the electrochemical cells (serpentine flow design or multiple parallel flow channels). With these complex flow fields there are composition variations along the length of the flow channel that will give rise to a variable current density, which make it difficult to recognize the effect that composition has on the current density (as shown in Figure 6); this in turn complicates the identification of the maximum in the energy efficiency. Our use of a stirred tank or differential cell permitted a direct connection between process parameters, flow rate, composition, temperature and applied potential, and hydrogen recovery and energy efficiency of the separation process. The key results from our studies are:

1. High purity hydrogen can be separated from CO_2 by electrochemical pumping. (This is in agreement with previous studies).

2. With Pt/C catalysts and mixtures of CO_2/H_2O and H_2, there is negligible activation overpotential for hydrogen oxidation at the anode or proton reduction at the cathode. (This is in agreement with previous studies).

3. At low applied potential difference ($V_{applied} < 0.5$ V) and hydrogen mole fraction at the anode >0.2, the current is limited by the potential applied across the polymer electrolyte membrane.

4. At moderate applied potential difference ($V_{applied} > 0.3$ V) and small hydrogen mole fraction at the anode $x^{anode}_{H2} < 0.1$, the current is limited by mass transport of hydrogen from the anode gas flow channel across the porous GDL to the anode catalyst layer.

5. The applied potential difference where the current transitions between proton transport limited and H_2 gas transport limited decreases as the mole fraction of hydrogen in the anode gas flow channel decreases.

6. The energy efficiency of hydrogen recovery is maximized when the applied potential difference corresponds to the transition between proton transport limited current and H_2 gas transport limited current.

The last four results provide the key connection between process parameters and hydrogen recovery and energy efficiency. This information can be used to develop models to design PEHPs for optimal performance.

The design and operation of a PEHP for hydrogen recovery involves a tradeoff between the efficiency of hydrogen recovery and the capital cost of the PEHP. By increasing the area of the membrane electrode assembly, the ohmic resistance for proton transport is decreased permitting more efficient operation. But the capital cost for the PEHP will increase with size because the cost of the catalyst and membrane make up the bulk of the cost of the separation unit. Recovery, $\mathcal{R}$, and throughput (hydrogen flow rate divided by MEA area) for are related by inequality 5.

$$\frac{F_{\mathrm{H,in}}^{\mathrm{anode}}}{A_{\mathrm{MEA}}k_{\mathrm{m}}(P_{\mathrm{T}}-P_{\mathrm{w}})} < \frac{1-\mathcal{R}}{\left[1+\left(C/H\right)_{\mathrm{in}}-\mathcal{R}\right]\mathcal{R}} \tag{5}$$

Increasing the recovery requires decreased flow per unit of MEA area. For 90% recovery of hydrogen with $(C/H)_{in} = 1$ and the gas diffusion electrodes used in our study ($k_m = 4.6 \times 10^{-5}$ mol/bar cm^2 s), the maximum current density ($F_{H,in}^{anode}/A_{MEA}$) is 0.4 A/cm^2.

Our studies reported here used a stirred tank or differential electrochemical cell where the compositions in the anode gas flow channel and cathode gas flow channel were uniform. The STR PEHP is a single stage separation unit. Changing the flow field design to serpentine or parallel flow channels is the equivalent of creating a multistage separation process. Multistage units can be modeled as single stage units placed in series or parallel. The experimental results with the single stage PEHP provide values of the membrane resistivity and GDL mass transport coefficient necessary to model multistage PEHPs and determine the optimal design and operation.

We present below a simple model of the PEHP based on the experimental results, and then apply the model to determine the optimal design and operation of hydrogen recovery units based on three different configurations of a PEHP: single stage, multistage with constant applied potential difference, and multistage with programmed applied potential difference.

Pumping of hydrogen across the membrane electrode assembly of the PEHP involves the sequence of transport and reaction steps outlined below:

1. Hydrogen gas molecules are transported by a combination of convection and diffusion across the anode GDL from the anode gas flow channel to the anode catalyst layer.
2. Hydrogen gas molecules are adsorbed on the anode catalyst.
3. Adsorbed hydrogen atoms are oxidized to protons and electrons.
4. Electrons move from the anode catalyst layer through the anode GDL, the external power supply, the cathode GDL to the cathode catalyst layer.
5. Protons move from the anode catalyst layer into and across the polymer electrolyte membrane.
6. Protons adsorb onto the cathode catalyst.
7. Protons and electrons combine making adsorbed hydrogen atoms at the cathode catalyst.
8. Hydrogen atoms recombine and desorb as H_2 molecules from the cathode catalyst.
9. H_2 gas molecules are transported by convection and diffusion across the cathode GDL to the cathode gas flow channel.

With good catalysts such as Pt the kinetics of hydrogen adsorption/desorption and hydrogen oxidation/reduction steps are rapid, and the rate limiting steps in hydrogen pumping will be the transport steps. There are also other transport steps occurring along with hydrogen pumping. Water will be transported across the membrane electrode assembly due to a concentration gradient. There will also be back diffusion of molecular hydrogen from the cathode to the anode. We will neglect those processes in the simplified model of the PEHP described below.

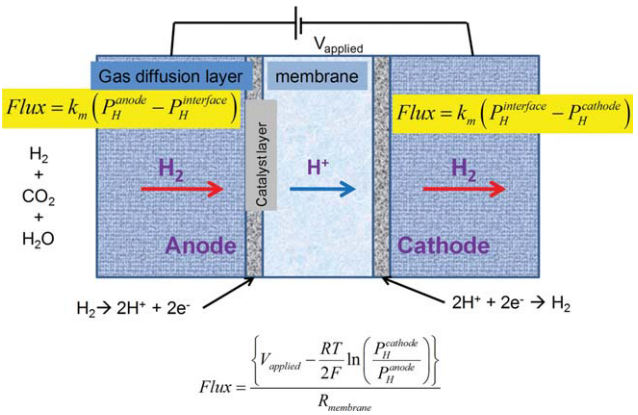

Figure 11. Schematic of the hydrogen flux across the gas diffusion electrodes and membrane in the polymer electrolyte hydrogen pump.

[Color figure can be viewed in the online issue, which is available at wileyonlinelibrary.com.]

Figure 11 is a schematic of the PEHP showing the driving forces for hydrogen transport across the gas diffusion electrodes and the polymer membrane. During steady-state operation, the hydrogen flux is the same across each of the three layers, as shown in Eq. 6. The catalyst layers are very thin and are assumed to have uniform composition. Hydrogen is transported across the anode GDL by both diffusion and bulk flow. The driving force for diffusion is the difference in hydrogen partial pressure between the anode gas flow channel and the anode catalyst layer. Bulk flow is driven by a small pressure differential between the anode gas flow channel and the anode catalyst layer created by removal of hydrogen at the catalyst layer by oxidation. The bulk flow at the anode carries both H_2 and CO_2 to the catalyst layer. As H_2 is removed by oxidation CO_2 accumulates, so the concentration of CO2 is greater at the anode catalyst layer than in the anode gas flow channel. At steady state, the convective flow of CO_2 to the anode catalyst layer must be balanced by CO_2 diffusion from the catalyst layer back to the anode gas flow channel. Because the bulk convective flow is balanced by the diffusive flow of CO_2 the hydrogen transport can be described by diffusion with a modified diffusion coefficient. In what follows, we chose to use a lumped mass transport coefficient, $k_m^{anode} \sim (D_{H_2}^{effective}\varepsilon/RT\tau t_{GDL})$, instead of introducing multiple unknown parameters for H_2 and CO_2 transport (the diffusivities of hydrogen, carbon dioxide and water, the porosity of the GDL, and the tortuosity of the GDL); such a simplified approach is sufficient for the present purpose.

At the cathode catalyst, protons and electrons recombine to make hydrogen gas resulting in a pressure differential across the cathode GDL. H_2 is convected across the cathode GDL. But, no diluent is convected with the H_2, so there is no back diffusion from the cathode gas flow channel to the catalyst layer. The resistance to the convective flow across the cathode GDL is small so the pressure differential is small and gas composition across the cathode GDL is nearly uniform. (We have estimated the pressure differential across the cathode GDL using Darcy's law to be ~100 Pa or 10^{-3} bar.) The hydrogen mass transport coefficient for the cathode (convective flow) is much greater than the hydrogen mass

transport coefficient for the anode (diffusive flow), $k_m^{\text{cathode}} \gg k_m^{\text{anode}}$.

The proton flux across the membrane is equal to the current, given by the voltage between the anode and cathode catalyst layers divided by the membrane resistance per unit membrane area (ρ_{mem}). The applied potential difference between the anode and cathode is opposed by the voltage associated with hydrogen's chemical potential difference between the anode and cathode catalyst layers (as distinguished from the hydrogen pressures in the gas flow channels). The opposing voltage corresponds to the work to raise the pressure of hydrogen from low pressure at the anode catalyst layer to high pressure at the cathode catalyst layer. The opposing voltage is the second term in the numerator of the current term in Eq. 6. The opposing voltage should also include the activation overpotential, but our experimental results with the Pt/C catalyst found that the activation overpotential was negligible.

$$\text{Flux} = k_m^{\text{anode}}\left\{P_H^{\text{anode}_{\text{channel}}} - P_H^{\text{anode}}\right\} = \frac{\left\{V_{\text{applied}} - \frac{RT}{2\mathcal{F}}\ln\left(\frac{P_H^{\text{cathode}}}{P_H^{\text{anode}}}\right)\right\}}{2\mathcal{F}\rho_{\text{mem}}} = k_m^{\text{cathode}}\left\{P_H^{\text{cathode}} - P_H^{\text{cathode}_{\text{channel}}}\right\} \quad (6)$$

The experiments revealed a change in the limiting transport resistance of hydrogen in the PEHP; at low concentrations of hydrogen in the anode feed and high voltages, the current is limited by mass transport across the anode GDL. The hydrogen concentration becomes depleted at the anode catalyst layer/membrane interface resulting in a large voltage opposing the applied potential difference. Equation 6 was solved numerically using the experimentally determined values of k_m and ρ_{mem} to determine the current as a function of the hydrogen partial pressure in the anode gas flow channel and applied potential difference and compared with the experimental data in Figure 6. The data could also be reasonably approximated by straight lines corresponding to the current increasing linearly with voltage at low applied potential differences a constant limiting current at larger applied potential differences. The linear approximation makes modeling much simpler, it only requires the partial pressures in the gas flow channels as inputs. The linear approximation captures the critical trends with reasonable accuracy to obtain semiquantitative comparisons of different system designs.

Operating at the transition between proton transport limited current and H_2 gas transport limited current is essential for efficient PEHP operation. When the current becomes H_2 gas transport limited, further increase in the applied potential difference does not produce any increase in current; hence, increasing voltage results in increased power dissipation without any increase in hydrogen recovery, and so the energy efficiency decreases. High energy efficiency requires the applied potential difference for the hydrogen pump be kept below the onset of the mass transport limiting current.

The optimal energy recovery efficiency with the minimum cost is achieved when operating at the H_2 gas transport limited current. This gives the highest throughput and recovery without energy dissipation due to mass transport across the anode GDL. The applied potential difference should be set to operate at the transition between ohmic control and mass transport control based on the composition in the anode gas flow channel, and the feed rate should be set to achieve maximum recovery at the mass transport limit. Increased voltages will result in dissipated energy without any increase hydrogen recovery. Increased feed rates will result in a smaller fraction of the hydrogen feed being recovered so the net energy efficiency also decreases.

The simple PEHP model consists of a set of mass balances at the anode, cathode, and across the MEA.

Mass balances at the anode

The flow rates in the analysis below are the molar flow rates per unit area of MEA (mol/cm^2/s), and j is the current density of protons.

$$\begin{aligned} F_{H_2,\text{out}}^{\text{anode}} &= F_{H_2,\text{in}}^{\text{anode}} - \frac{j}{2\mathcal{F}} \\ F_{CO_2,\text{out}}^{\text{anode}} &= F_{CO_2,\text{in}}^{\text{anode}} \\ F_{H_2O,\text{out}}^{\text{anode}} &= F_{H_2O,\text{in}}^{\text{anode}} \end{aligned} \quad (7)$$

Mass balance at cathode

The flow out of the cathode is equal to half the proton current across the electrolyte membrane. We have neglected any crossover by diffusion or electro-osmotic drag; these are small secondary effects.

$$F_{H_2,\text{out}}^{\text{cathode}} = \frac{j}{2\mathcal{F}} \quad (8)$$

The current density is determined by the balance of the hydrogen fluxes across the membrane and the anode GDL as shown in Figure 11. The simplified linear model of the current density in the PEHP given by Eq. 9 was used in the calculations. Equation 9 neglects both the activation overpotential and the opposing potential generated between the anode and cathode catalyst layers due to depletion of hydrogen at the anode. The experimental data showed the activation overpotential was negligible ($\eta_{\text{act}} < 0.01$ V). The depletion voltage is only important there is severe mass transport limitations across the anode GDL, for example, $(P_{H_2}^{\text{anode}_{\text{channel}}}/P_{H_2}^{\text{anode}_{\text{catalyst}}} > 100)$, corresponding to voltages $\sim$0.2 V greater than the transition voltage; as the optimal design condition is at or close to the transition voltage, we need not concern ourselves with the depletion voltage in our simplified analysis.

At low applied potential differences, the current is equal to the applied potential difference between the anode and cathode divided by the areal membrane resistance, ρ_{mem}. (ρ_{mem} is the effective resistance combining both membrane resistance and the ohmic resistance of the ionomer in the catalyst layer). At high applied potential difference, the current density is constant at the H_2 gas transport limited current. The transition to the H_2 gas transport limited current depends on the mole fraction of hydrogen in the anode flow channel.

$$j = \begin{cases} \frac{V_{\text{applied}}}{\rho_{\text{mem}}} & \frac{V_{\text{applied}}}{\rho_{\text{mem}}} < j_{\max} \\ j_{\max} = 2\mathcal{F}k_m x_{H_2,\text{out}}^{\text{anode}} P_T & \frac{V_{\text{applied}}}{\rho_{\text{mem}}} > j_{\max} \end{cases} \quad (9)$$

The mole fraction of hydrogen at the anode is given by Eq. 10, where the pressure ratio term accounts for the dilution by water vapor. Equation 10 assumes the anode to behave as a perfectly mixed unit, and the composition in the anode flow channel is uniform and the same as the effluent. It is also assumed that the anode effluent is saturated with water vapor; as seen in our experiments, some condensation of water can occur, but, in our simple analysis, we do not track it. (Analyzing water condensation and its influence on the hydrogen transport are important if we are able to analyze the oscillations reported in Figures 4 and 7.)

$$x_{H_2}^{anode} = \frac{F_{H_2,out}^{anode}}{F_{H_2,out}^{anode} + F_{CO_2,out}^{anode} + F_{H_2O,out}^{anode}} = \frac{F_{H_2,out}^{anode}}{\left(F_{H_2,out}^{anode} + F_{CO_2,out}^{anode}\right)\left(\frac{P^{anode}}{P^{anode} - P_{H_2O}^{0}}\right)} \quad (10)$$

Equations 7, 8, and 10 can be substituted into the Eq. 9 to solve for the maximum current density.

$$\frac{j_{max}}{2\mathcal{F}} = \frac{1}{2}\left\{\left[F_{CO_2,in}^{anode} + F_{H_2,in}^{anode}\right]\frac{P}{P - P_{H_2O}^{0}} + k_m P\right\} - \frac{1}{2}\left\{\left(\left[F_{CO_2,in}^{anode} + F_{H_2,in}^{anode}\right]\frac{P}{P - P_{H_2O}^{0}} + k_m P\right)^2 - 4k_m P F_{H_2,in}^{anode}\right\}^{1/2} \quad (11)$$

Hydrogen recovery and energy efficiency can be determined using Eqs. 5 and 6 (substituting current density for current). The applied potential difference for the maximum current density is found from $V_{applied} = j_{max}\rho_{mem}$. Experimental data were presented here for Pt/C coated Nafion 115 membrane with E-Tek porous GDL electrodes found $\rho_{mem} = 0.47\ \Omega\ cm^2$ and $k_m = 2.4 \times 10^{-5}$ mol/bar cm^2 s. Hydrogen recovery and energy efficiency as functions of applied potential difference predicted by this simplified model are compared with the experimental data in Figure 9. The data at other flow rates and temperatures were fit equally well with this model (not shown). The bilinear approximation of the simplified model results in sharp maximum in efficiency as a function of applied potential difference; a more refined model could better fit the experimental data, but the simplified model considered in this study makes it easier to identify the controlling physics of the PEHP operation.

The model presented above is for a single stage PEHP, analogous to a flash drum or condenser for vapor/liquid separations. The recovery and energy efficiency as a function of the inlet molar flow per unit of MEA area are shown in Figure 12. At the experimental conditions reported here, the maximum energy efficiency was ~45%. However, model analysis reveals that by decreasing the flow rate per unit area of the MEA, it is possible to increase the recovery and energy efficiency; the energy efficiency can be increased to over 65% by decreasing the flow per unit MEA area by a factor of 2.

The efficiency maxima occur when the recovery causes the current to reach the mass transport limit. Inset in Figure 12 is the applied potential difference as a function of the

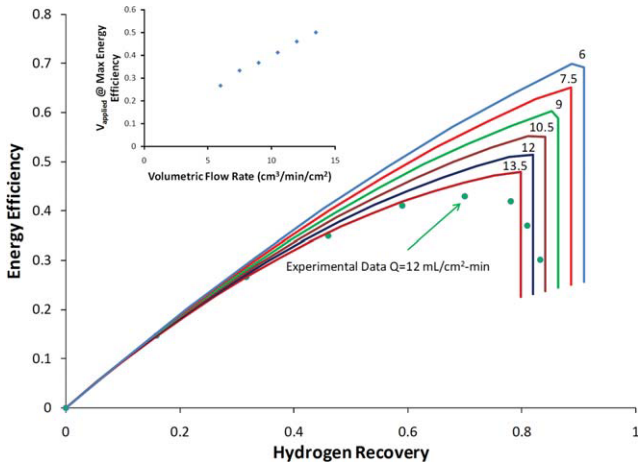

Figure 12. Efficiency vs. Hydrogen Recovery as a function of feed flow rate per unit MEA area.

The family of curves are for $(C/H)_{in} = 0.5$ with water saturated feeds at 50°C and flow rates of 6–13.5 mL/cm^2 min. The points are the experimental data for 12 mL/min feed. The inset graph is the applied potential difference at the maximum energy efficiency. [Color figure can be viewed in the online issue, which is available at wileyonlinelibrary.com.]

feed flow rate; the optimum applied potential difference must be reduced at low feed flow rates. As the inlet flow rate is reduced, the hydrogen mole faction at the anode of the PEHP is reduced because a larger fraction of the hydrogen in pumped from the anode to the cathode. At lower hydrogen mole fraction at the anode the H_2 gas transport limited current occurs at lower values. Figure 12 reflects the same trends seen experimentally in Figure 9, and higher energy efficiency can be achieved by reducing the feed flow per unit area of MEA. Figure 12 suggests that energy efficiency in a single stage separation unit can be improved from 40% to over 60% by reducing the flow rate per unit area by a factor of 2. This illustrates the PEHP operation is similar to other separation processes—higher efficiency is achieved at reduced throughput.

Further improvement to the efficiency of the PEHP can be achieved with a multistage process. Multiple stages can be obtained with either distinct units or flow channels that reduce axial mixing (thereby creating the equivalent of multiple units). Multistage processes can be modeled as a series of single stage separation units, with each stage having an effective resistance, $R_{stage} = \rho_{mem}/A_{stage}$, and mass transport coefficient $k_{stage} = k_m \times A_{stage}$. Two methods of operation can be considered, either constant applied potential difference (same $V_{applied}$ for each stage) or a programmed voltage ($V_{applied}$ can be optimized for each stage).

First, consider multistage operation with fixed applied potential difference. At the inlet to the PEHP, the hydrogen pressure is high, and the current will be limited by the applied potential difference. As hydrogen is depleted along the length of the flow channel, the mass transport of hydrogen across the porous GDL electrode becomes progressively limiting. If the applied potential difference is the same for every stage, at some stage, the hydrogen mole fraction will be reduced to the point where there is a transition from proton transport limited current to H_2 gas transport limited

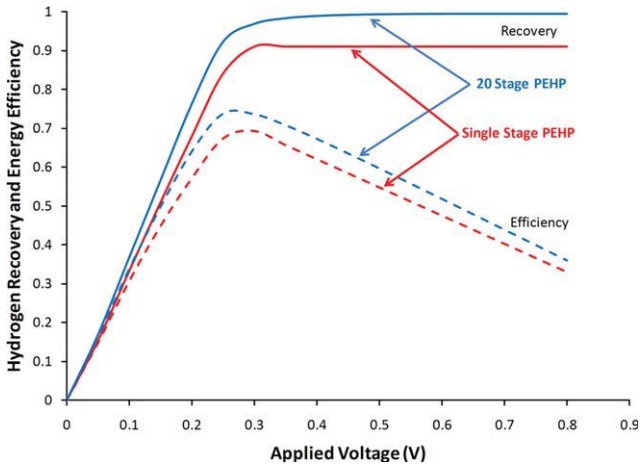

Figure 13. Efficiency and recovery of a single stage and multistage (20 stage) PEHP for hydrogen recovery from $(C/H)_{in}=0.5$ $CO_2/H_2/H_2O$ mixture at a feed rate of 6.3 cm^3/cm^2 min.

The multistage unit is the same total size as the single stage unit. [Color figure can be viewed in the online issue, which is available at wileyonlinelibrary.com.]

current. Stages downstream of this transition will operate in the H_2 gas transport limited current regime and have lower energy efficiency. The optimal energy efficiency of a fixed voltage multistage unit occurs, when the feed flow rate is adjusted so the transition to H_2 gas transport limited current occurs at final stage. The applied potential difference limits the hydrogen mole fraction in the anode outlet, which limits the maximum hydrogen recovery and energy efficiency. The

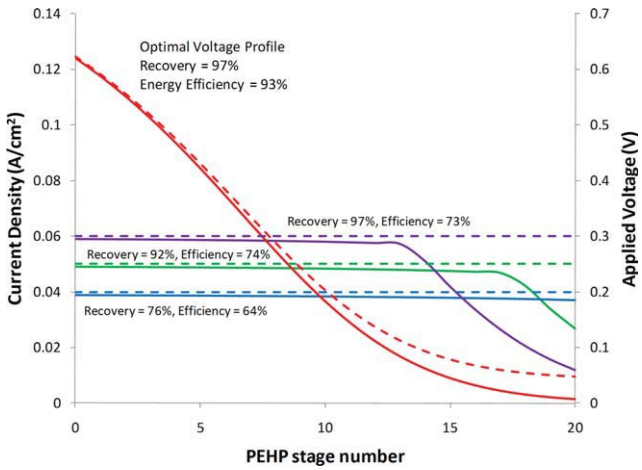

Figure 14. Voltage and current along the length of a 20 stage PEHP separating a $CO_2/H_2/H_2O$ mixture at 50°C.

The solid lines are the current density in each stage and the dashed lines are the voltage in each stage. The voltage programmed unit has a voltage profile chosen such that the unit always operates at the maximum voltage where ohmic reistance is current limiting. At fixed voltage the current is limited by ohmic resistance near the inlet but becomes H_2 gas transport limited as hydrogen is depleted causing the current density to decrease. As the voltage increases the depletion zone moves towards the inlet. [Color figure can be viewed in the online issue, which is available at wileyonlinelibrary.com.]

maximum energy efficiency of a fixed voltage 20 stage PEHP with $(C/H)_{in} = 0.5$ was estimated in our study to be circa 74%.

The hydrogen recovery and energy efficiency for a 20-stage PEHP with constant voltage is compared with a single stage PEHP with the same total MEA area and flow rate in Figure 13. The multistage system achieves higher efficiency because it operates over a larger region with voltage limiting the current. The multistage unit achieves maximum efficiency at slightly lower applied potential difference than the single stage unit.

Higher overall energy efficiency can be obtained if each stage of the PEHP is operated at maximum efficiency. This requires programming the voltage to each stage of the PEHP so that the applied potential difference corresponds to the transition voltage for the local composition at that stage, i.e. the applied potential difference is adjusted to always have operation at the transition between proton transport limited current and H_2 gas transport limited current. Voltage programming could be accomplished with segmented electrodes along straight parallel flow channels. With a multistage unit the voltage is set highest at the inlet where the mole fraction of hydrogen is highest. As hydrogen is depleted in each stage the voltage is decreased to always stay in the proton transport limited current regime. The maximum energy efficiency of a variable voltage 20 stage PEHP with $(C/H)_{in} = 0.5$ is circa 93%.

Figure 14 compares 20-stage PEHPs with fixed voltage and programmed voltage. By programming the voltage to always be at the transition between proton transport limited current and H_2 gas transport limited current at the local concentration the overall energy efficiency is substantially increased. Table 1 compares the optimal performance of a single stage PEHP with multistage PEHPs with either fixed or programmed voltages. The results in Table 1 show that the energy efficiency can be substantially improved through the use of a programmed voltage. The model for the PEHP shows that the system can be designed and operated to achieve high recovery (>90%) with high net energy efficiency (>90%). The voltage programmed multistage PEHP can, in theory, achieve greater efficiency than amine scrubbing. A more complete economic analysis is required to assess whether the improved efficiency can justify the capital cost for this technology.

The major advantages to the PEHP are: (1) the hydrogen stream has high purity and is not contaminated—other processes recover a purified CO_2 stream and the hydrogen requires additional purification; (2) the hydrogen is recovered as a pressurized stream—the PEHP does the pumping and additional pumping is not required; (3) the process does not require high temperature or pressure making it simpler and

Table 1. Efficiency of Operation of a PFR Hydrogen Pump

Voltage	Hydrogen Recovery (%)	Energy Efficiency (%)
Single stage $V_{applied} = 0.45$ V	62.3	44.2
20 Stage, fixed $V_{applied} = 0.2$ V	76.3	64.1
20 Stage, fixed $V_{applied} = 0.25$ V	92.2	73.8
20 Stage, fixed $V_{applied} = 0.3$ V	96.8	73.6
20 Stage, variable $V_{applied} = 0.65 \rightarrow 0.02$	98.25	92.6

safer; (4) the process is inherently modular and could be adopt for distributed processing.

The most important result for the design of PEHPs is that mass transport across the GDL is often the dominant resistance for proton current and accounts for much of the energy losses in hydrogen purification. Reducing the membrane resistance certainly improves the energy efficiency when the PEHP is operated where the applied potential difference is current limiting, but energy losses because of the mass transport resistance are the dominant energy loss at high hydrogen recovery.

Conclusions

The recovery and energy efficiency of hydrogen separation from a simulated reformate stream with a PEHP was measured as functions of the operating parameters: gas flow rate, gas composition, temperature, and applied potential difference. Hydrogen was recovered in a single stage PEHP with very high purity (>99.99%) at energy efficiencies of 45%. The hydrogen current in the PEHP was limited by the applied potential difference at low applied potential differences and high hydrogen mole fraction in the feed. As hydrogen is depleted through pumping, the current becomes limited by mass transport across the porous GDL at the anode. When the current is H_2 gas transport limited, the energy efficiency of the PEHP is reduced. Optimal separation performance is achieved when the applied potential difference is at the transition between proton transport limited current and mass transport limited current. The key engineering parameters for the hydrogen pump are the membrane resistance and the mass transport coefficient for the GDL at the anode. These were measured for a Nafion-based PEHP.

The experimental results formed the basis for predictive models of single stage and multistage PEHPs for hydrogen recovery from reformate streams. A simple model is able to reasonably fit the experimental data and was extended to demonstrate that energy efficiencies of >90% with >98% hydrogen recovery are possible with voltage programmed multistage PEHPs.

Acknowledgments

The authors thank the NSF (CBET 0754715) for support of this work. Ahmed Abdulla thanks the Alder Senior Thesis fund administered by Princeton University's School of Engineering and Applied Sciences for partial support of this work. Kathryn Laney thanks the Princeton University Grand Challenge for fund, and Miriam Padilla thanks the NSF (DMR) for REU support of this work. The authors thank May Jean Cheah for her assistance in preparing membrane electrodes used in this work.

Notation

A_{MEA} = area of membrane electrode assembly (cm)
$D_{H2}^{effective}$ = effective diffusion coefficient of hydrogen in the GDL
$F_{i,location}^{electrode}$ = molar flow of species i at inlet or outlet location at the anode or cathode (mol/s), also used for areal flow rates (mol/cm^2 s)
F_{dry} = molar flow of hydrogen and carbon dioxide to the anode (mol/s)
$R_{membrane}$ = membrane resistance (Ω)
i = proton current (amp)
i_{max} = maximum current = 2(hydrogen feed rate)
j = current density (amp/cm^2)
k_m = mass transport coefficient (mol/bar cm^2)
ρ_{mem} = areal resistivity of membrane (Ω cm^2)
$V_{applied}$ = voltage applied between the anode and cathode (volt)
P_w = water vapor pressure (bar)
P_w^0 = saturation water vapor pressure at pump temperature (bar)
P_T = Total Pressure (bar)
P_H = hydrogen pressure (bar)
P_{CO_2} = carbon dioxide pressure (bar)
$\mathcal{R}$ = hydrogen recovery
R = gas constant
t_{GDL} = thickness of gas diffusion layer
x_H = hydrogen mole fraction
x_C = carbon dioxide mole fraction
ε = void fraction of GDL
$\mathcal{F}$ = Faraday's constant (96,468 coulombs/mol)
$\Delta H_{combustion}$ = heat of combustion of hydrogen (286 kJ/mol)
η_{act} = activation overpotential for hydrogen oxidation/reduction
τ = tortuosity of GDL

Literature Cited

1. Baade WF, Parekh UN, Raman VS. *Hydrogen. Kirk-Othmer Encyclopedia of Chemical Technology*, Vol. 13. New York: Wiley, 2004:759–808.
2. Holladay JD, Hu J, King DL, Wang Y. An overview of hydrogen production technologies. *Catal Today*. 2009;139:244–260.
3. National Hydrogen Association; Hydrogen. Clean Energy for the Future. 2010; Available at: http://www.hydrogenassociation.org/. Accessed Sept. 15, 2010.
4. U.S. Department of Energy Hydrogen Program. 2010; Available at: http://www.hydrogen.energy.gov/production.html. Accessed Sept. 15, 2010.
5. Department of Energy. Hydrogen from Coal Research. Available at: http://www.fossil.energy.gov/programs/fuels/hydrogen/Hydrogen_from_Coal_R%26D.html. Accessed Sept. 15, 2010.
6. U.S. Department of Energy. Carbon Sequestration R&D. Available at: http://fossil.energy.gov/programs/sequestration/overview.html. Accessed Sept. 15, 2010.
7. Perinline HW, Luebke DR, Jones KL, Myers CR, Morsi BI, Heintz YJ, Ilconich JB. Progress in carbon dioxide capture and separation research for gasification-based power generation point sources. *Fuel Process Technol*. 2008;89:897–907.
8. Rochelle GT. Amine scrubbing for CO2 capture. *Science*. 2009;325:1652–1654.
9. Lee KB, Beaver MG, Caram HS, Sircar S. Reversible chemisorption of carbon dioxide: simultaneous production of fuel-cell grade H-2 and compressed CO2 from synthesis gas. *Adsorption*. 2007;13:385–397.
10. Yang SI, Choi DY, Jang SC, Kim SH, Choi DK. Hydrogen separation by multi-bed pressure swing adsorption of synthesis gas. *Adsorption*. 2008;14:583–590.
11. Iyuke SE, Daud WRW, Mohamad AB, Kadhum AAH, Fisal Z, Shariff AM. Application of Sn-activated carbon in pressure swing adsorption for purification of H-2. *Chem Eng Sci*. 2000;55:4745–4755.
12. Ribeiro AM, Grande CA, Lopes FVS, Loureiro JM, Rodrigues AE. A parametric study of layered bed PSA for hydrogen purification. *Chem Eng Sci*. 2008;63:5258–5273.
13. Ho MT, Allinson GW, Wiley DE. Reducing the cost of CO2 capture from flue gases using pressure swing adsorption. *Ind Eng Chem Res*. 2008;47:4883–4890.
14. Ritter JA, Ebner AD. State-of-the-art adsorption and membrane separation processes for hydrogen production in the chemical and petrochemical industries. *Separ Sci Technol*. 2007;42:1123–1193.
15. Tagliabue M, Delnero G. Optimization of a hydrogen purification system. *Int J Hydrogen Energy*. 2008;33:3496–3498.
16. Czaja AU, Trukhan N, Muller U. Industrial applications of metal-organic frameworks. *Chem Soc Rev*. 2009;38:1284–1293.
17. Li JR, Kuppler RJ, Zhou HC. Selective gas adsorption and separation in metal-organic frameworks. *Chem Soc Rev*. 2009;38:1477–1504.

18. Adhikari S, Fernando S. Hydrogen membrane separation techniques. *Ind Eng Chem Res*. 2006;45:875–881.
19. Phair JW, Donelson R. Developments and design of novel (non-palladium-based) metal membranes for hydrogen separation. *Ind Eng Chem Res*. 2006;45:5657–5674.
20. Tosti S. Supported and laminated Pd-based metallic membranes. *Int J Hydrogen Energy*. 2003;28:1445–1454.
21. Brown I, Bowden M, Kemmitt T, Wu J, Carvalho J. Nanostructured alumina ceramic membranes for gas separation. *Int J Mod Phys B*. 2009;23:1015–1020.
22. Frost CB, Robinson M. The application of ultra-thin palladium alloy metal foils in gas-phase hydrogen separation or purification. *JOM*. 2007;59:63–64.
23. Nishimura C, Komaki M, Hwang S, Amano M. V-Ni alloy membranes for hydrogen purification. *J Alloys Compd*. 2002;330:902–906.
24. Lu GQ, da Costa JCD, Duke M, Giessler S, Socolow R, Williams RH, Kreutz T. Inorganic membranes for hydrogen production and purification: a critical review and perspective. *J Colloid Interface Sci*. 2007;314:589–603.
25. Ryi SK, Park JS, Kim SH, Cho SUH, Hwang KR, Kim DW, Kim HG. A new membrane module design with disc geometry for the separation of hydrogen using Pd alloy membranes. *J Membr Sci*. 2007;297:217–225.
26. Sircar S, Golden TC. Purification of hydrogen by pressure swing adsorption. *Sep Sci Technol*. 2000;35:667–687.
27. Song CS. Fuel processing for low-temperature and high-temperature fuel cells—challenges, and opportunities for sustainable development in the 21st century. *Catal Today*. 2002;77:17–49.
28. Ghenciu AF. Review of fuel processing catalysts for hydrogen production in PEM fuel cell systems. *Curr Opin Solid State Mater Sci*. 2002;6:389–399.
29. Haruta M. Gold as a novel catalyst in the 21st century: preparation, working mechanism and applications. *Gold Bull*. 2004;37:27–36.
30. Manasilp A, Gulari E. Selective CO oxidation over Pt/alumina catalysts for fuel cell applications. *Appl Catal B-Environ*. 2002;37:17–25.
31. Trimm DL, Onsan ZI. Onboard fuel conversion for hydrogen-fuel-cell-driven vehicles. *Catal Rev-Sci Eng*. 2001;43:31–84.
32. Korotkikh O, Farrauto R. Selective catalytic oxidation of CO in H-2: fuel cell applications. *Catal Today*. 2000;62:249–254.
33. Rohland B, Eberle K, Strobel R, Scholta J, Garche J. Electrochemical hydrogen compressor. *Electrochim Acta*. 1998;43:3841–3846.
34. Barbir F, Gorgun H. Electrochemical hydrogen pump for recirculation of hydrogen in a fuel cell stack. *J Appl Electrochem*. 2007;37:359–365.
35. Sedlak JM, Austin JF, Laconti AB. Hydrogen recovery and purification using the solid polymer electrolyte electrolysis cell. *Int J Hydrogen Energy*. 1981;6:45–51.
36. Gardner CL, Ternan M. Electrochemical separation of hydrogen from reformate using PEM fuel cell technology. *J Power Sources*. 2007;171:835–841.
37. Casati C, Longhi P, Zanderighi L, Bianchi F. Some fundamental aspects in electrochemical hydrogen purification/compression. *J Power Sources*. 2008;180:103–113.
38. Perry KA, Eisman GA, Benicewicz BC. Electrochemical hydrogen pumping using a high-temperature polybenzimidazole (PBI) membrane. *J Power Sources*. 2008;177:478–484.
39. LLC HP. 2008; Available at: http://h2pumpllc.com/index.html. Accessed Sept. 15, 2010.
40. Eisman G. *Integrated Electrochemical Hydrogen Separation Systems*. US: H2 Pump LLC, 2007.
41. Benziger J, Chia E, Karnas E, Moxley J, Teuscher C, Kevrekidis IG. The stirred tank reactor polymer electrolyte membrane fuel cell. *AIChE J*. 2004;50:1889–1900.

Manuscript received Feb. 8, 2010, and revision received Aug. 6, 2010.